J. Fluid Mech. (1997), *vol.* 331, *pp.* 405–428

Absolute instability of the Ekman layer and related rotating flows

By R. J. LINGWOOD

Department of Engineering, University of Cambridge, Trumpington Street, Cambridge CB2 1PZ, UK

(Received 7 June 1996 and in revised form 20 September 1996)

This paper is concerned with the theoretical behaviour of the laminar Ekman layer and the family of related rotating problems that includes both the Bödewadt and the von Kármán boundary-layer flows. Results from inviscid and viscous analyses are presented. In both cases, within specific regions of the parameter space, it is shown that the flows are absolutely unstable in the radial direction, i.e. disturbances grow in time at every radial location within these regions. Outside these regions, the flows are convectively unstable or stable. The absolute or convective nature of the flows is determined by examining the branch-point singularities of the dispersion relation. The onset of absolute instability is consistent with available experimental observations of the onset of laminar–turbulent transition in these flows.

1. Introduction

F. Nansen observed that the drift of surface ice was angled at 20–40° to the right of the wind direction (in the northern hemisphere), and correctly attributed this effect to the fact that the Coriolis forces introduced by the rotation of the Earth are not negligible compared to the slow drift velocities. Based on this suggestion, Ekman (1905) analysed the problem of a wind-driven rotating flow, resulting from balanced pressure gradient, Coriolis and frictional forces. Ekman showed that the flow has a boundary-layer structure, within which the mean velocity can be represented by a vector that changes length exponentially with depth and changes angle linearly with depth; the so-called Ekman spiral.

Although boundary-layer velocity profiles that approximate to the Ekman layer occur in the atmospheric boundary layer and in wind-driven surface layers of the ocean, turbulence always plays a role in atmospheric and oceanic boundary layers because of rough boundary surfaces. Unsteadiness of the mean flow and thermal effects may also be important. Here, only steady laminar mean flows will be considered, but the following study of rotating boundary-layer flows may have applications to geophysical flows. The similarities between the laminar Ekman layer and the von Kármán boundary layer (the steady axisymmetric incompressible flow due to an infinite disk rotating in still fluid; von Kármán 1921) are well established; see, for example, Tatro & Mollö-Christensen (1967), Faller (1991), Lingwood (1995). The susceptibility of both these flows to inviscid crossflow instability (often referred to as type-1 instability) is to be expected from the similarly inflectional mean velocity component. Crossflow instability was first noticed by Smith (1947) in the rotating-disk flow and then by Gray (1952) in the flow over a swept wing, where it manifested itself as a striped pattern fixed to the wing surface consisting of a series of stationary vortices

in the boundary layer. Evidence of crossflow instability of the von Kármán and Ekman boundary layers is given by Gregory, Stuart & Walker (1955) and Faller (1963), respectively. Both these flows also have a second convectively unstable mode, which is often referred to as a type-2 mode, that is dominant at low Reynolds numbers and stable in the inviscid limit.

The recent theoretical study of the stability of the von Kármán boundary layer by Lingwood (1995) discovered an absolute instability, produced by a coalescence of the inviscidly unstable mode and a third mode that is spatially damped and inwardly propagating. The absolute instability has been confirmed experimentally by Lingwood (1996*a*) and it is suggested that this instability mechanism is responsible for the onset of nonlinear behaviour and laminar–turbulent transition. This discovery, and the general similarities between the von Kármán and the Ekman boundary layers, prompted the study presented here. As discussed by Huerre & Monkewitz (1990), the response of the flow to impulsive forcing shows whether it is convectively or absolutely unstable. If the response to the transient disturbance grows with time at a fixed location in space, then the flow is absolutely unstable. Following the work of Briggs (1964) and Bers (1975) in the field of plasma physics, absolute instability can be identified by singularities in the dispersion relationship that occur when modes associated with waves propagating in opposite directions coalesce. Such points have become known as pinch points. It is usual in linear stability analysis to choose either temporal or spatial theories. Temporal theory assumes that the disturbances grow or decay with time from an initial spatial distribution. This implies that the wavenumber is real and that the frequency is complex. Spatial theory, however, assumes that the frequency is real and that the wavenumber is complex. Thus, the disturbances evolve in space from an initial temporal distribution. Where absolute instability is suspected it is necessary to perform a spatio-temporal analysis.

Both the linear Ekman layer and the von Kármán flow are exact solutions of the Navier–Stokes equations, which is an attractive feature for theoretical analyses. The Ekman layer has the further advantage that it is strictly parallel. Both flows have constant boundary-layer thicknesses and are therefore parallel in the physical sense but, while the von Kármán boundary layer has a Reynolds number that varies with radius (due to the radius-dependent characteristic velocity), the Ekman layer can have constant geostrophic velocity giving a single Reynolds-number definition of the flow. Thus, the need to account for downstream growth of the boundary layer or to make a local parallel-flow approximation to reduce the governing partial differential equations to a more amenable ordinary differential set is unnecessary. Therefore, the Ekman layer makes a good model flow for theoretical studies. Experimentally, an Ekman layer can be established by modifying the von Kármán flow with the introduction of a geostrophic velocity in the main body of the fluid. If the fluid at infinity is in rigid-body rotation, then the linear Ekman layer is approached as the differential rotation rate between the disk and the body of fluid becomes small compared with the system rotation rate, because it is in this limit that the nonlinear inertial forces are negligible compared to the Coriolis forces, and the radius simultaneously tends to large values to maintain a geostrophic flow. If the fluid at infinity is a potential vortex, sustained by an applied radial pressure gradient, then again the linear Ekman layer is approached as the nonlinear inertial forces become negligible compared to the Coriolis forces, which requires that the product of the radius and rotation rate is much larger than the geostrophic velocity. In either case the geostrophic velocity is dependent on the radius, the flow is no longer defined by a single Reynolds number, and is therefore no longer strictly parallel.

Faller (1963) and Tatro & Mollö-Christensen (1967) carried out experiments, in which a rotating fluid contained a sink on the central axis of rotation and distributed sources round the outer edge. Further experimental and theoretical studies of the motion produced by sources and sinks in a fluid rotating about a vertical axis in a tank were performed by Barcilon (1967) and Hide (1968). If there is a closed curve in the plane perpendicular to the axis of rotation through which there is a net flux of mass, Hide (1968) showed that the net transport of fluid occurs within both the Stewartson sidewall layers (Stewartson 1957) and the horizontal-wall layers, having an Ekman-layer structure. These experiments showed the presence of instability waves in the Ekman layers, where the Rossby number (the ratio of convective to Coriolis terms) was small, which have been successfully analysed by neglecting the nonlinear inertial terms from the mean flow equations and assuming a constant geostrophic velocity (Lilly 1966; Faller & Kaylor 1966; Spooner & Criminale 1982; Marlatt & Biringen 1994). Marlatt & Biringen (1995) describe a numerical simulation of secondary instability of the type-2 mode.

Batchelor (1951) discussed qualitatively, and Rogers & Lance (1960) and Faller (1991) obtained solutions for, the mean flow of a wide class of boundary-layer flows established between a fluid at infinity in a state of rigid-body rotation and a surface with a differential rotation rate. Particular cases of this family of flows are the Bödewadt, Ekman and von Kármán boundary-layer flows. As mentioned above, the Ekman layer is produced in this family of flows when the boundary and the fluid at infinity approach the same rotation rate and the radius tends to infinity. Bödewadt (1940) studied the flow produced over an infinite stationary plane in fluid rotating with uniform angular velocity at an infinite distance from the plane; a problem that has an exact solution of the Navier–Stokes equations for the mean flow. In the von Kármán boundary-layer flow, fluid is thrown radially outwards due to the action of centrifugal forces and is replaced by a downwards axial flow. On the other hand in the Bödewadt flow, there is an equilibrium of centrifugal and radial pressure-gradient forces in the fluid rotating an infinite distance above the plane but the centrifugal forces are reduced within the boundary layer, due to viscous action, and the axially independent radial pressure gradient causes a radial flow that is predominantly inwards and a consequent (from continuity arguments) upwards axial flow.

The structure of the paper is as follows. A brief description of the linear Ekman layer solution of the Navier–Stokes equations for the mean flow is given in §2. An analysis of the family of flows with the main body of fluid in rigid-body rotation is given in §3, followed by the results in §4, and concluding remarks are given in §5.

2. The Ekman layer

Ekman (1905) considered the flow in terms of a constant eddy viscosity, but the analysis is directly applicable to laminar flows by replacing the eddy viscosity with a constant dynamic viscosity. Furthermore, the analysis can be applied to a layer above a rigid boundary (to suit an atmospheric flow above the Earth's surface), as well as to one below a free surface. For example, consider a large body of fluid at rest relative to a uniformly rotating boundary that is set into motion by a uniform pressure gradient (modified to incorporate effects of gravity and centrifugal force), which is then balanced by the Coriolis force. If the pressure gradient lies in the (x^*,y^*)-plane (where the plane rotates about the z^*-axis at angular velocity Ω^*, and asterisks will henceforth be used to denote dimensional quantities) with components $(P_x^*, 0)$, then the equations giving the mean velocity components (U^*,V^*) in the Ekman layer near

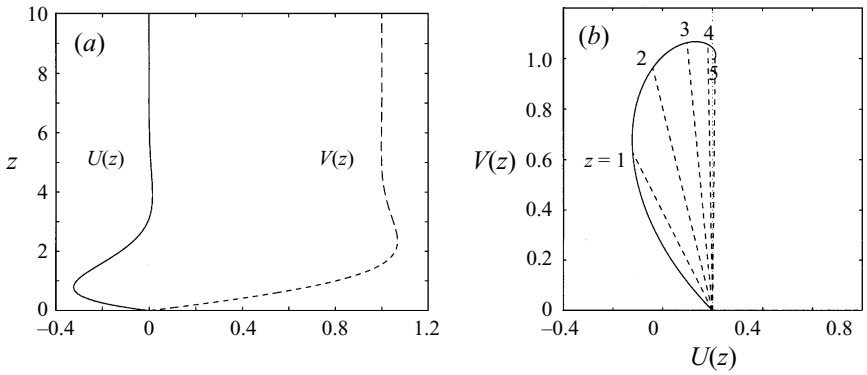

FIGURE 1. (*a*) Mean velocity profiles for the Ekman layer flow. (*b*) Mean velocity profiles plotted as an Ekman spiral.

the boundary ($z^* = 0$) are

$$-2\Omega^* V^* = -\frac{P_x^*}{\rho^*} + \nu^* \frac{\partial^2 U^*}{\partial z^{*2}}, \tag{2.1}$$

$$2\Omega^* U^* = \nu^* \frac{\partial^2 V^*}{\partial z^{*2}}, \tag{2.2}$$

where ρ^* and ν^* are the fluid density and kinematic viscosity, respectively. There are no-slip boundary conditions at $z^* = 0$ and the geostrophic velocity at large z^* is $V^*(z^* \to \infty) \equiv V_\infty^* = P_x^*/(2\rho^*\Omega^*)$. The non-dimensionalized analytic solution to (2.1)–(2.2) is

$$U(z) = \frac{U^*}{V_\infty^*} = -\mathrm{e}^{-z}\cos z, \tag{2.3}$$

$$V(z) = \frac{V^*}{V_\infty^*} = 1 - \mathrm{e}^{-z}\cos z, \tag{2.4}$$

where $z = z^*/l^*$ and $l^* = (\nu^*/\Omega^*)^{1/2}$. Figure 1 shows the mean velocity components plotted against the axial coordinate in (*a*) and as an Ekman spiral in (*b*). The velocity near $z = 0$ is linear in z and inclined at 45° in a clockwise direction from the direction of the body force due to the applied pressure gradient.

The Reynolds number for this flow is

$$Re = \frac{V_\infty^* l^*}{\nu^*} = \frac{P_x^*}{2\rho^*\Omega^*(\Omega^*\nu^*)^{1/2}}. \tag{2.5}$$

The non-dimensional Navier–Stokes equation, in a frame rotating at Ω^*, and continuity equation are

$$\frac{\partial \tilde{\boldsymbol{U}}}{\partial t} + (\tilde{\boldsymbol{U}}\cdot\nabla)\tilde{\boldsymbol{U}} + \frac{2}{Re}\boldsymbol{k}\wedge\tilde{\boldsymbol{U}} = -\nabla\tilde{P} + \frac{1}{Re}\nabla^2\tilde{\boldsymbol{U}}, \tag{2.6}$$

$$\nabla\cdot\tilde{\boldsymbol{U}} = 0. \tag{2.7}$$

Here, t is time, $\tilde{\boldsymbol{U}} = [\tilde{U},\ \tilde{V},\ \tilde{W}]^T$ where the components of the vector are the instantaneous velocities each composed from a sum of the mean velocity and a small perturbation velocity, $\tilde{P}$ is the instantaneous pressure, $\boldsymbol{k}$ is the unit vector in the z-direction and ∇^2 is the Laplacian operator. The non-dimensionalizing velocity,

pressure and time scales are V_∞^*, $\rho^* V_\infty^{*2}$ and l^*/V_∞^*, respectively. Subtracting the mean flow from (2.6), linearizing with respect to the perturbation quantities and neglecting terms of order Re^{-2} and higher results in equations that are separable in x, y and t (without any parallel-flow approximation) and perturbation quantities that can be expressed in normal-mode form

$$[u,\ v,\ w,\ p]^T = [\hat{u}(z),\ \hat{v}(z),\ \hat{w}(z),\ \hat{p}(z)]^T \mathrm{e}^{\mathrm{i}(\alpha x+\beta y-\omega t)} + \text{c.c.} \tag{2.8}$$

Here, for example, $\hat{u}$ is the spectral representation of the perturbation u, α and β are the wavenumbers in the x- and y-directions, respectively, ω is the disturbance frequency and c.c. denotes complex conjugate. The perturbation equations are

$$\mathrm{i}\hat{u}(-\omega+\alpha U+\beta V)+U'\hat{w}-2\hat{v}/Re=-\mathrm{i}\alpha\hat{p}-(\gamma^2\hat{u}-\hat{u}'')/Re, \tag{2.9}$$

$$\mathrm{i}\hat{v}(-\omega+\alpha U+\beta V)+V'\hat{w}+2\hat{u}/Re=-\mathrm{i}\beta\hat{p}-(\gamma^2\hat{v}-\hat{v}'')/Re, \tag{2.10}$$

$$\mathrm{i}\hat{w}(-\omega+\alpha U+\beta V)=-\hat{p}'-(\gamma^2\hat{w}-\hat{w}'')/Re, \tag{2.11}$$

$$\mathrm{i}(\alpha\hat{u}+\beta\hat{v})+\hat{w}'=0, \tag{2.12}$$

where $\gamma^2=\alpha^2+\beta^2$ and primes denotes differentiation with respect to z.

3. The theoretical model for the BEK flows

The model presented here describes a family of boundary-layer flows caused by a differential rotation rate between a solid boundary, or disk, and an incompressible fluid in rigid-body rotation above (see Faller 1991). As mentioned in §1, particular cases of this family are the Bödewadt, Ekman and von Kármán boundary-layer flows; hence, this family will be referred to as the BEK system. The radius of the disk and the extent of the fluid above the disk are considered to be infinite, and the disk and fluid rotate about the same vertical axis with angular velocities Ω_D^* and Ω_F^*, respectively. The Bödewadt layer arises when the disk is stationary and the fluid rotates, i.e. $\Omega_D^*=0$ and $\Omega_F^*\neq 0$, for the Ekman layer $\Omega_D^*\approx\Omega_F^*$ and for the von Kármán layer (the 'rotating-disk' boundary-layer flow described by Lingwood 1995, 1996*a*) $\Omega_D^*\neq 0$ and $\Omega_F^*=0$. Between these particular examples are flows in which both the disk and the fluid rotate, but with differing angular velocities. Although the model is valid for counter- and co-rotating systems, only co-rotating systems will be analysed here.

The continuity and momentum equations for the axisymmetric mean flow are formulated in cylindrical-polar coordinates r^*, θ and z^*, in a frame rotating at Ω_D^*, and can be written as

$$\frac{1}{r^*}\frac{\partial(r^*U^*)}{\partial r^*}+\frac{\partial W^*}{\partial z^*}=0, \tag{3.1}$$

$$U^*\frac{\partial U^*}{\partial r^*}+W^*\frac{\partial U^*}{\partial z^*}-\frac{V^{*2}}{r^*}-2\Omega_D^*V^* = -\frac{1}{\rho^*}\frac{\partial P^*}{\partial r^*}+\nu^*\left(\frac{1}{r^*}\frac{\partial}{\partial r^*}\left(r^*\frac{\partial U^*}{\partial r^*}\right)+\frac{\partial^2U^*}{\partial z^{*2}}-\frac{U^*}{r^{*2}}\right), \tag{3.2}$$

$$U^*\frac{\partial V^*}{\partial r^*}+W^*\frac{\partial V^*}{\partial z^*}-\frac{U^*V^*}{r^*}+2\Omega_D^*U^*=\nu^*\left(\frac{1}{r^*}\frac{\partial}{\partial r^*}\left(r^*\frac{\partial V^*}{\partial r^*}\right)+\frac{\partial^2V^*}{\partial z^{*2}}-\frac{V^*}{r^{*2}}\right), \tag{3.3}$$

$$U^*\frac{\partial W^*}{\partial r^*}+W^*\frac{\partial W^*}{\partial z^*}=\nu^*\left(\frac{1}{r^*}\frac{\partial}{\partial r^*}\left(r^*\frac{\partial W^*}{\partial r^*}\right)+\frac{\partial^2W^*}{\partial z^{*2}}\right), \tag{3.4}$$

where U^*, V^* and W^* denote the mean radial, azimuthal and axial velocities, respectively, and P^* is the mean pressure. By extension of the exact similarity solution to the Navier–Stokes equations for the von Kármán flow (von Kármán 1921), it is assumed that the dimensionless mean flow variables have the following form:

$$U(z) = \frac{U^*}{r^*\Delta\Omega^*} = \frac{U^*}{r^*\Omega^* Ro}, \tag{3.5}$$

$$V(z) = \frac{V^*}{r^*\Delta\Omega^*} = \frac{V^*}{r^*\Omega^* Ro}, \tag{3.6}$$

$$W(z) = \frac{W^*}{l^*\Delta\Omega^*} = \frac{W^*}{l^*\Omega^* Ro}, \tag{3.7}$$

$$P(r,z) = \frac{P^*}{\rho^* l^{*2}\Delta\Omega^{*2}} = \frac{P^*}{\rho^* l^{*2}\Omega^{*2} Ro^2}. \tag{3.8}$$

Here, $\Delta\Omega^* = \Omega_F^* - \Omega_D^*$, r and z are the dimensionless forms of r^* and z^*, where $l^* = (\nu^*/\Omega^*)^{1/2}$ is the non-dimensionalizing length scale, Ω^* is a system rotation rate and Ro is the Rossby number, which is a constant of the flow. The Rossby number and Ω^*, respectively, are defined as

$$Ro = \frac{\Delta\Omega^*}{\Omega^*}, \tag{3.9}$$

$$\Omega^* = \frac{\Omega_F^*}{2 - Ro} + \frac{\Omega_D^*}{2 + Ro} = \frac{\Omega_F^* + \Omega_D^*}{4} + \left(\left(\frac{\Omega_F^* + \Omega_D^*}{4} \right)^2 + \frac{(\Delta\Omega^*)^2}{2} \right)^{1/2}. \tag{3.10}$$

So, for example, for the Bödewadt layer $Ro = 1$ and $\Omega^* = \Omega_F^*$, for the Ekman layer $Ro = 0$ and $\Omega^* = \Omega_F^* = \Omega_D^*$, and for the von Kármán layer $Ro = -1$ and $\Omega^* = \Omega_D^*$.

Substituting (3.5)–(3.8) into (3.1)–(3.4) gives the following non-dimensional equations for the mean flow:

$$2U + H' = 0, \tag{3.11}$$

$$Ro(U^2 + WU' - (V^2 - 1)) - Co(V - 1) - U'' = 0, \tag{3.12}$$

$$Ro(2UV + WV') + CoU - V'' = 0, \tag{3.13}$$

$$Ro(WW' + P') - H'' = 0, \tag{3.14}$$

where the prime denotes differentiation with respect to z and $Co = 2\Omega_D^*/\Omega^* = 2 - Ro - Ro^2$ is a Coriolis parameter. Figure 2 shows Co plotted against Ro; Co is equal to 2 for the von Kármán and the Ekman layers, but $Co = 0$ for the Bödewadt layer. This figure also gives the ratio Ω_F^*/Ω_D^* for $-1 \leqslant Ro \leqslant 1$, which tends to infinity as $Ro \to 1$. To formulate (3.12) it is necessary to determine the radial pressure gradient that appears in (3.2) from the relative circumferential flow as $z \to \infty$, i.e. $V \to 1$. By assuming that $U(z \to \infty) = U'(z \to \infty) = U''(z \to \infty) = 0$, (3.2) gives

$$Ro + Co = \frac{1}{\rho^*\Omega^{*2} r^* Ro} \frac{\partial P^*}{\partial r^*}, \tag{3.15}$$

which is taken as a constant in z. Thus, the mean pressure has the form

$$P^* = \rho^*\Omega^{*2} l^{*2} Ro^2 \left(\frac{r^2(Ro + Co)}{2Ro} + P(z) + \text{const.} \right). \tag{3.16}$$

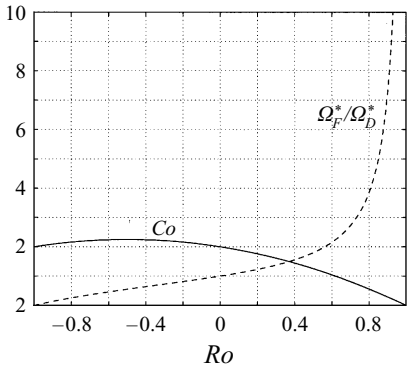

FIGURE 2. Variation in Co and Ω_F^*/Ω_D^* with Ro for the BEK system.

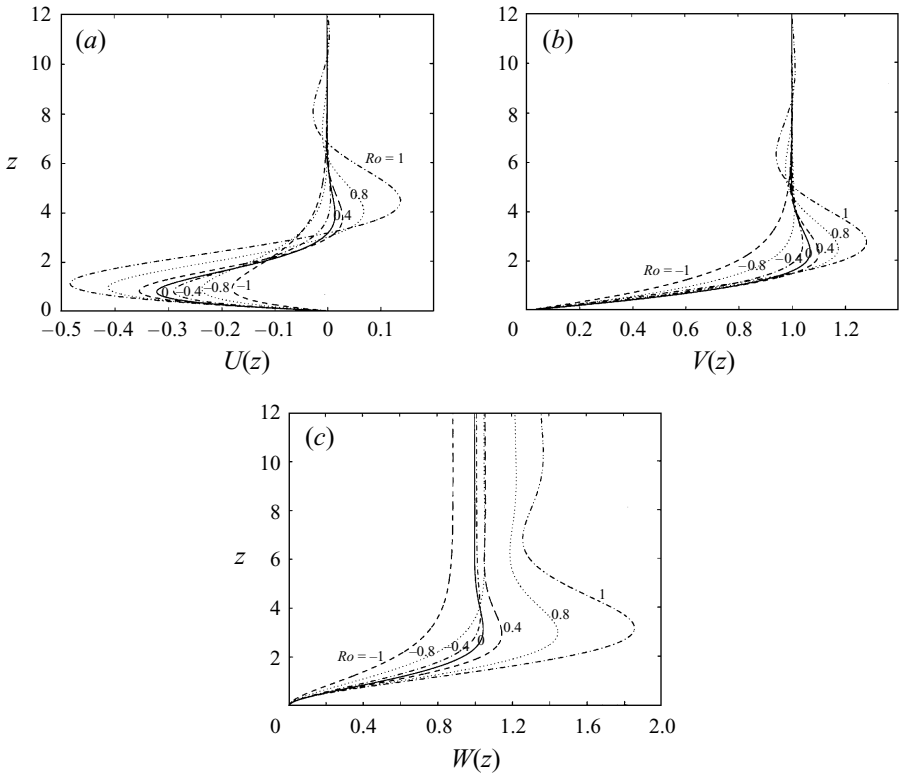

FIGURE 3. Mean velocity profiles for the BEK flows: (*a*) radial, (*b*) circumferential, (*c*) axial.

Equations (3.11)–(3.14) are solved subject to the boundary conditions

$$U(0) = V(0) = W(0) = 0, \tag{3.17}$$

$$U(z \to \infty) = 0, \qquad V(z \to \infty) = 1. \tag{3.18}$$

A double-precision fourth-order Runge–Kutta integrator and a Netwon–Raphson searching method were used to solve the set of ordinary differential equations (3.11)–(3.14) for $U(z)$, $V(z)$, $W(z)$ and $P(z)$. Figure 3 shows U, V and W plotted against z for a range of Ro from -1 to 1. For the von Kármán flow, i.e. $Ro = -1$, only the

Ro	$U'(0)$	$V'(0)$
−1.0	−0.5102	0.6159
−0.8	−0.6855	0.7699
−0.6	−0.8090	0.8701
−0.4	−0.8977	0.9375
−0.2	−0.9599	0.9797
0.0	−1.000	1.000
0.2	−1.0205	1.0000
0.4	−1.0229	0.9794
0.6	−1.0082	0.9372
0.8	−0.9783	0.8703
1.0	−0.9420	0.7729

TABLE 1. Values of U' and V' at $z = 0$ for various Ro, which are needed to calculate the mean velocity profiles.

radial mean velocity profile is inflectional, but the azimuthal and axial profiles also become inflectional with increasing Rossby number; for $Ro = 1$, U, V and W are all inflectional. The sign of the dimensional velocities U^*, V^* and W^* depends on the sign of Ro. For Ro exactly zero, (3.7) and (3.8) show that $W^* = P^* = 0$, whereas U^* and V^* are non-zero because $r^* \to \infty$ as $Ro \to 0$ such that the denominators of (3.5) and (3.6) are non-zero. These zero-Rossby-number solutions of the BEK system are equivalent to the linear Ekman layer described in §2. The values of U' and V' at $z = 0$ are given in table 1 to four decimal places for a range of Ro. Note that where comparisons can be made between these tabulated values and previously calculated values they agree. For example, these quantities are given for $Ro = -1$ in Schlichting (1979), where tabulated values of U, V and W are also given for the Bödewadt layer.

A linear stability analysis is applied at a radius r_a^*, by imposing infinitesimally small disturbances on the mean flow. The local Reynolds number is Re, where

$$Re = \frac{r_a^* \Delta\Omega^* l^*}{\nu^*} = r_a Ro, \tag{3.19}$$

and the non-dimensionalizing velocity, pressure and time scales are $r_a^*\Omega^* Ro$, $\rho^* r_a^{*2}\Omega^{*2}Ro^2$ and $l^*/(r_a^*\Omega^* Ro)$, respectively. Clearly, for negative Rossby number the Reynolds number is also negative, but this is purely a result of considering positive- and negative-Rossby-number flows in a single model, and the results presented in §4 will be in terms of positive Re (where the magnitude is taken for flows with negative Rossby number) for all Ro. The instantaneous non-dimensional velocities and pressure are given by

$$\bar{u}(r,\theta,z,t) = \frac{rRo}{Re}U(z) + u(r,\theta,z,t), \tag{3.20}$$

$$\bar{v}(r,\theta,z,t) = \frac{rRo}{Re}V(z) + v(r,\theta,z,t), \tag{3.21}$$

$$\bar{w}(r,\theta,z,t) = \frac{Ro}{Re}W(z) + w(r,\theta,z,t), \tag{3.22}$$

$$\bar{p}(r,\theta,z,t) = \frac{Ro^2}{Re^2}P(r,z) + p(r,\theta,z,t), \tag{3.23}$$

where u, v, w and p are small perturbation quantities.

The dimensionless Navier–Stokes equations, in cylindrical-polar coordinates ro-

tating at Ω_D^*, are linearized with respect to the perturbation quantities. In order to make the linearized equations separable in r, θ and t, it is necessary to ignore variations in the Reynolds number with radius. This approximation, which is often called the parallel-flow approximation, involves replacing the variable r that appears in the coefficients of the linearized equations by the local Reynolds number Re. Terms $O((Ro/Re)^2)$ are neglected and the perturbation quantities are assumed to have normal-mode form, for example

$$u = \hat{u}(z;\alpha,\beta,\omega;Re,Ro)\mathrm{e}^{\mathrm{i}(\alpha r+\bar{\beta}\theta-\omega t)} + \text{c.c.}, \tag{3.24}$$

where $\hat{u}$ is the spectral representation of the radial perturbation velocity, α and $\bar{\beta} = \beta Re/Ro$ are the radial and azimuthal wavenumbers, respectively, ω is the frequency of the disturbance in a frame rotating at Ω_D^*, and c.c. denotes complex conjugate. In the analysis of negative-Rossby-number flows, owing to the Rossby number in the non-dimensionalizing time scale, ω takes the opposite sign to ω^*. However, in §4 the results are presented with ω and ω^* having the same sign as each other for all Ro. Because of the circumferential periodicity of these flows the quantity $\bar{\beta}$ takes integer values. Similar equations to (3.24) define $\hat{v}$, $\hat{w}$ and $\hat{p}$.

The perturbation equations may be written as a set of six first-order ordinary differential equations in the following transformed variables:

$$\left.\begin{array}{ll} \phi_1 = \bar{\alpha}\hat{u} + \beta\hat{v}, & \phi_2 = \bar{\alpha}\hat{u}' + \beta\hat{v}', \\ \phi_3 = \hat{w}, & \phi_4 = \hat{p}, \\ \phi_5 = \bar{\alpha}\hat{v} - \beta\hat{u}, & \phi_6 = \bar{\alpha}\hat{v}' - \beta\hat{u}', \end{array}\right\} \tag{3.25}$$

where $\bar{\alpha} = \alpha - \mathrm{i}Ro/Re$. The perturbation equations are

$$\phi_1' = \phi_2, \tag{3.26}$$

$$\phi_2' = (\gamma^2 + \mathrm{i}Re(\alpha U + \beta V - \omega) + RoU)\phi_1 + RoW\phi_2 + (\bar{\alpha}U' + \beta V')Re\phi_3 + \mathrm{i}\bar{\gamma}^2 Re\phi_4 - (2RoV + Co)\phi_5, \tag{3.27}$$

$$\phi_3' = -\mathrm{i}\phi_1, \tag{3.28}$$

$$\phi_4' = \mathrm{i}RoW\phi_1/Re - \mathrm{i}\phi_2/Re - (\gamma^2 + \mathrm{i}Re(\alpha U + \beta V - \omega) + RoW')\phi_3/Re, \tag{3.29}$$

$$\phi_5' = \phi_6, \tag{3.30}$$

$$\phi_6' = (2RoV + Co)\phi_1 + (\bar{\alpha}V' - \beta U')Re\phi_3 + \beta Ro\phi_4 + (\gamma^2 + \mathrm{i}Re(\alpha U + \beta V - \omega) + RoU)\phi_5 + RoW\phi_6, \tag{3.31}$$

where $\gamma^2 = \alpha^2 + \beta^2$ and $\bar{\gamma}^2 = \alpha\bar{\alpha} + \beta^2$.

If the Coriolis and streamline curvature effects are neglected, the result can be written as a fourth-order equation

$$(\alpha U + \beta V - \omega)(\phi_3'' - \gamma^2\phi_3) - (\alpha U'' + \beta V'')\phi_3 + \mathrm{i}(\phi_3'''' - 2\gamma^2\phi_3'' + \gamma^4\phi_3)/Re = 0, \tag{3.32}$$

and a coupled second-order equation

$$(\alpha U + \beta V - \omega)\phi_5 - \mathrm{i}(\alpha V' + \beta U')\phi_3 + \mathrm{i}(\phi_5'' - \gamma^2\phi_5)/Re = 0, \tag{3.33}$$

where the vertical vorticity component $\phi_5 = \alpha\hat{v} - \beta\hat{u}$, rather than the definition in (3.25), because of the neglect of streamline curvature terms. If all terms of $O(Ro/Re)$ are also neglected and viscosity is considered to act only in the establishment of the mean flow, equation (3.32) reduces to

$$(\alpha U + \beta V - \omega)(\phi_3'' - \gamma^2\phi_3) - (\alpha U'' + \beta V'')\phi_3 = 0. \tag{3.34}$$

Note that (3.32), (3.33) and (3.34) are extensions of the usual Orr–Sommerfeld, Squire and Rayleigh equations, respectively.

To distinguish between a convectively and an absolutely unstable response, the governing equations, whether viscous or inviscid, are solved subject to an impulsive azimuthal line forcing, with prescribed integer $\bar{\beta}$ such that the vertical velocity at $z = 0$ is given by

$$\hat{w}(0; r, \theta, t) = \delta(r - r_a)\delta(t)\mathrm{e}^{\mathrm{i}\bar{\beta}\theta}, \tag{3.35}$$

where $\delta(r - r_a)$ and $\delta(t)$ are the Dirac delta functions at r_a and $t = 0$, respectively. The response to point forcing can be obtained by summing over all integer values of $\bar{\beta}$. Where appropriate, the additional boundary conditions at $z = 0$ given by the no-slip condition are

$$\hat{u}(0; r, \theta, t) = \hat{v}(0; r, \theta, t) = 0, \tag{3.36}$$

and as $z \to \infty$ it is required that all perturbations decay.

The following assumes a viscous analysis, but it also applies to an inviscid analysis if the Reynolds-number dependence is dropped. Solution of an inhomogeneous system such as this is described in detail in Lingwood (1997), but suffice it to say that the problem reduces to solving a Green's function of the form

$$w(z; r, \theta, t) = \frac{\mathrm{e}^{\mathrm{i}\bar{\beta}\theta}}{(2\pi)^2} \int_F \int_A \frac{\Phi(z; \alpha, \omega; \beta, Re, Ro)}{\Delta_0(\alpha, \omega; \beta, Re, Ro)} \mathrm{e}^{\mathrm{i}(\alpha(r - r_a) - \omega t)} \mathrm{d}\alpha \mathrm{d}\omega, \tag{3.37}$$

where Φ is a function of z formed from a combination of the independent solution vectors of the governing ordinary differential equations (see Lingwood 1997), $\Delta_0 = 0$ is the dispersion relation, which is satisfied by the discrete eigenvalues of the homogeneous problem (the unforced case) and A and F are inversion contours in the α- and ω-planes, respectively. The discrete eigenvalues provide a mapping between the α- and ω-planes, such that zeros of the dispersion relation in the α-plane are given by

$$\alpha = \alpha_j(\omega, \beta; Re, Ro), \quad j = 1, \ldots, M, \tag{3.38}$$

and in the ω-plane zeros are given by

$$\omega = \omega_j(\alpha, \beta; Re, Ro), \quad j = 1, \ldots, N, \tag{3.39}$$

where M and N are the number of discrete modes in the α- and ω-planes, respectively. Discrete eigenvalues trace out paths in the α-plane (ω-plane) as ω (α) is varied. Trajectories in the α-plane given by a predetermined ω-distribution (possibly complex) will be referred to as spatial branches of the dispersion relation. Similarly, trajectories in the ω-plane given by a predetermined α-distribution (possibly complex) will be referred to as temporal branches. Note that the governing equations have a symmetry property, whereby $\alpha_j(\omega, \beta; Re, Ro) \mapsto -\alpha_j^*(-\omega^*, -\beta^*; Re, Ro)$ and $\omega_j(\alpha, \beta; Re, Ro) \mapsto -\omega_j^*(-\alpha^*, -\beta^*; Re, Ro)$, where the asterisks indicate the complex conjugate. Thus, trajectories of the dispersion relation given by (3.38) for $\omega_r < 0$ and $\beta_r < 0$ (henceforth, the subscripts r and i will be used for real and imaginary parts, respectively) are symmetric with respect to the imaginary α-axis to those for $\omega_r > 0$ and $\beta_r > 0$. Similarly, trajectories given by (3.39) for $\alpha_r < 0$ and $\beta_r < 0$ are symmetric about the imaginary ω-axis to those for $\alpha_r > 0$ and $\beta_r > 0$.

Briggs' method (Briggs 1964) is used to calculate the time-asymptotic discrete solution, due to the discrete poles of (3.37) (i.e. zeros of the dispersion relation). Details of this method are given in Lingwood (1997), where it is shown that the discrete response is sufficient to determine the nature of the instability. The discrete

response to (3.37) neglects the continuous contributions from branch cuts in the α-plane, which give the z-structure of the response close to the source of the initial perturbation and are caused by the complex square-roots taken to satisfy the boundary conditions as $z \to \infty$.

For fixed $\bar{\beta}$, Briggs' criterion for absolute instability requires a branch-point singularity between two, or more, spatial branches of the dispersion relation, of which at least two must lie in distinct halves of the α-planes when ω_i is sufficiently large and positive. Such singularities have become known as pinch points because inherent in Briggs' method is the use of analytic continuation to deflect the inversion contours, and at these singularities the A-contour becomes pinched between the coalescing spatial branches. The pinching frequency ω^o is a branch point of the function $\alpha(\omega; \beta, Re, Ro)$ or, equivalently, α at the pinch point, α^o, is a saddle point of the function $\omega^o(\alpha; \beta, Re, Ro)$ and at this point $\partial\omega/\partial\alpha = 0$, although this condition is not sufficient for such points. If $\omega_i > 0$ at the pinch point the flow is absolutely unstable, otherwise the flow is only convectively unstable or stable. A branch-point singularity between two spatial branches that originate in the same half of the α-plane for large positive ω_i does not constitute a pinch point (even though $\partial\omega/\partial\alpha = 0$ at such a point) and does not cause an absolute instability. This sort of branch point results in a second-order pole, which leads to transient algebraic growth that can be important if the second-order pole is near neutral but ultimately behaves exponentially as dictated by the sign of α_i. This case will not be pursued here, but further details can be found in Koch (1986) and Henningson & Schmid (1992).

The governing equation for the inviscid linear stability analysis is the Rayleigh equation (3.34) and it has singularities at critical points, where $\alpha U(z_c) + \beta V(z_c) - \omega = 0$. The Rayleigh equation has amplified and damped solutions in complex conjugates pairs. However, physically relevant solutions match on to the solutions of the viscous equations for large Reynolds number. Lin (1945*a*,*b*,*c*) showed that to get the appropriate solutions, the path of integration must pass under the singularity if $\bar{U}'(z_c) > 0$, where $\bar{U} = (\alpha U + \beta V)/(\alpha^2 + \beta^2)^{1/2}$, or over the singularity if $\bar{U}'(z_c) < 0$. Following a method developed by Healey (1996), this condition was satisfied by calculating $\bar{U}(z)$ and $\bar{U}''(z)$ for complex values of z. The eigenvalues were found using a double-precision fixed-step-size fourth-order Runge–Kutta integrator (using a path of integration that always passed on the correct side of singularities in the inviscid case) and a Newton–Raphson linear search procedure. Gram–Schmidt orthonormalization was used in the viscous analysis.

4. Results and discussion

The linear Ekman layer, which is described in §2, can be subjected to viscous and inviscid stability analyses in the way described in the preceding section. That is, the perturbation equations (2.9)–(2.12) can be written as six first-order ordinary differential equations using the transformations given in (3.25) for the BEK system or, neglecting viscous and Coriolis effects, they can be written as the Rayleigh equation. The resulting equations can then be used to investigate the discrete time-asymptotic impulse response to distinguish between convective and absolute instability as described in §3. Figure 4 shows branches of the dispersion relation in the complex ω- and α-planes for the linear Ekman layer. In this case, α is the wavenumber in the x-direction, i.e. perpendicular to the geostrophic flow, and β is the wavenumber in the y-direction, i.e. parallel to the geostrophic flow. Figure 4(*a*) shows results from a purely inviscid analysis and figure 4(*b*) shows similar results from a sixth-order

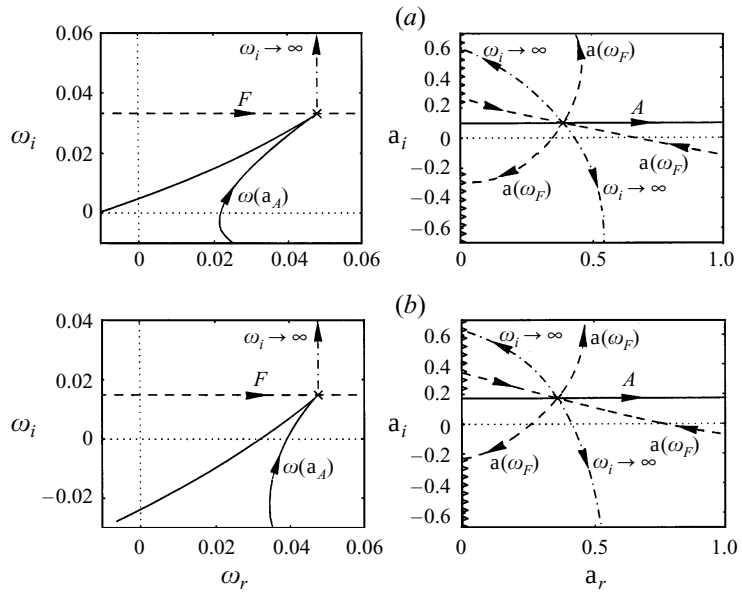

FIGURE 4. (*a*) Inviscid temporal branch in the ω-plane (given by the A-contour) and the inviscid spatial branches in the α-plane (given by the F-contour) for $Ro = 0$ and $\beta = 0.14$. (*b*) Viscous temporal branch in the ω-plane (given by the A-contour) and the viscous spatial branches in the α-plane (given by the F-contour) for $Re = 566$, $Ro = 0$ and $\beta = 0.14$. Imaginary-axis branch cuts in the α-plane are indicated by zigzag lines, ω^o and α^o are marked by $\times$ and the mapping of $\omega = \omega^o + \mathrm{i}\omega_i$, where $\omega_i \to \infty$, is shown in the α-plane (— · — ·).

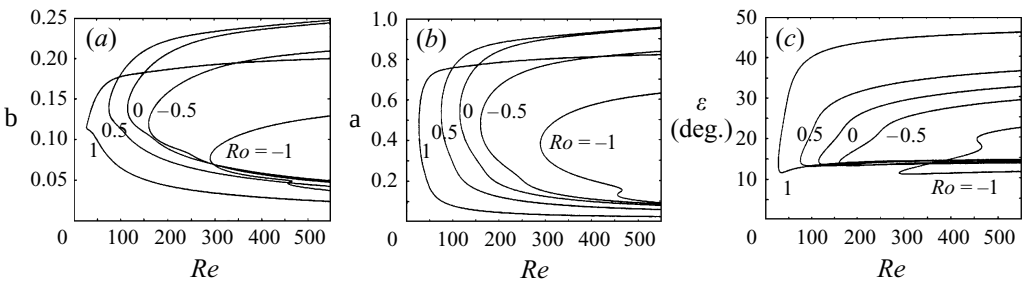

FIGURE 5. Neutral-stability curves ($\omega_i = \alpha_i = 0$) for stationary waves ($\omega_r = 0$) for the BEK system. The convectively unstable regions lie within the curves.

viscous analysis, which includes Coriolis effects, at the same value of β as (*a*) and at $Re = 566$. In both cases, there is a pinch point with positive ω_i^o, which implies that both are absolutely unstable in the x-direction. The pinch points occur due to a coalescence between a spatially growing branch (for x less than x at the source) and a spatially decaying branch (for x greater than x at the source). These branches separate into the distinct halves of the α-plane as $\omega_i \to \infty$, which qualifies the branch points as pinch points. Furthermore, paths in the α-plane that pass through the pinch points form cusps at the branch points in the ω-plane. This is a characteristic of a pinch point that has been used by Kupfer, Bers & Ram (1987) to identify points of absolute instability. The values of α^o in the inviscid and viscous examples are very similar, as is ω_r^o, but ω_i^o is significantly greater in the inviscid case. This is to be expected from the absolute instability results for the von Kármán flow (Lingwood 1995), where

Ro	*Re*	α	β	ε (deg.)
−1.0	290.1	0.381	0.077	11.4
−0.5	160.9	0.467	0.117	14.1
0.0	116.3	0.528	0.137	14.5
0.5	75.9	0.544	0.140	14.4
1.0	27.4	0.487	0.115	13.3

TABLE 2. Approximate values of *Re*, α, β and ε at the noses of the marginal curves for stationary waves in figure 5.

the degree of absolute instability (the size of ω_i^o) increases with Reynolds number. As with the von Kármán boundary layer, the viscous results presented in figure 4(*b*) approach the inviscid results in figure 4(*a*) at large Reynolds number, and the inviscid branches are the asymptotic limits of the viscous branches. These results also correspond exactly to the zero-Rossby-number solution of the BEK system (discussed below), where α and β revert to their definitions in §3: the radial and circumferential wavenumbers, respectively.

Figure 5 shows marginal curves for convective instability of stationary modes, i.e. disturbances with $\omega = 0$, for various Rossby numbers in the BEK system. In figure 5(*c*) the curves are plotted against the wave angle $\varepsilon = \tan^{-1}(\beta/\alpha_r)$. The curves for $Ro = -1$ are essentially the same as those presented in figure 6(*b*) of Lingwood (1995). Clearly, as the Rossby number increases from the von Kármán layer to the Bödewadt layer the stationary modes become increasingly unstable. As discussed in Lingwood (1995), the marginal curves for the von Kármán flow consist of two branches: branch 1 is inviscidly unstable and branch 2 is a balance between viscous and Coriolis forces. For other Rossby numbers the curves also consist of two branches. For flows with negative Rossby number the two convectively unstable branches can be shown by causality arguments only to exist outwards from the source, i.e. for $r > r_a$, whereas for flows with positive Rossby number the two convectively unstable branches exist inwards from the source ($r < r_a$). For the Ekman layer, the behaviour of the two branches follows the negative-Rossby-number flows if $Ro = 0^-$, i.e. if Ω_F^* tends to Ω_D^* from below and the radial mean velocity is directed predominantly outwards, and follows the positive-Rossby-number flows if $Ro = 0^+$, i.e. if Ω_F^* tends to Ω_D^* from above and the radial mean velocity is directed predominantly inwards. The marginal curves change with non-zero frequency. It has been shown by Lilly (1966) and Melander (1983) that the most unstable mode for the Ekman layer is a travelling branch-2 mode with a critical Reynolds number of about 55 ($\varepsilon \approx 7.5°$) and 54.2 ($\varepsilon \approx 7.2°$), respectively, compared with Lilly's calculation of about 115 (116 in this study) for the onset of (branch-1) stationary waves. The critical Reynolds number for convective instability of stationary waves in the Ekman layer agrees quite closely with experimentally observed Reynolds numbers of about 125 (Faller & Kaylor 1966). The instabilities in the Ekman layer observed by Faller & Kaylor (1966) had a wave angle of about 14°, which is consistent with the stationary branch-1 inviscidly unstable waves. Tatro & Mollö-Christensen (1967) observed branch-1 modes in the Ekman layer with almost constant wave angle of 14.6°. Thus, although branch-2 travelling waves can have significantly lower critical Reynolds numbers than stationary waves, it is the latter that are more commonly observed in experiments. This fact could be due to greater receptivity of the boundary

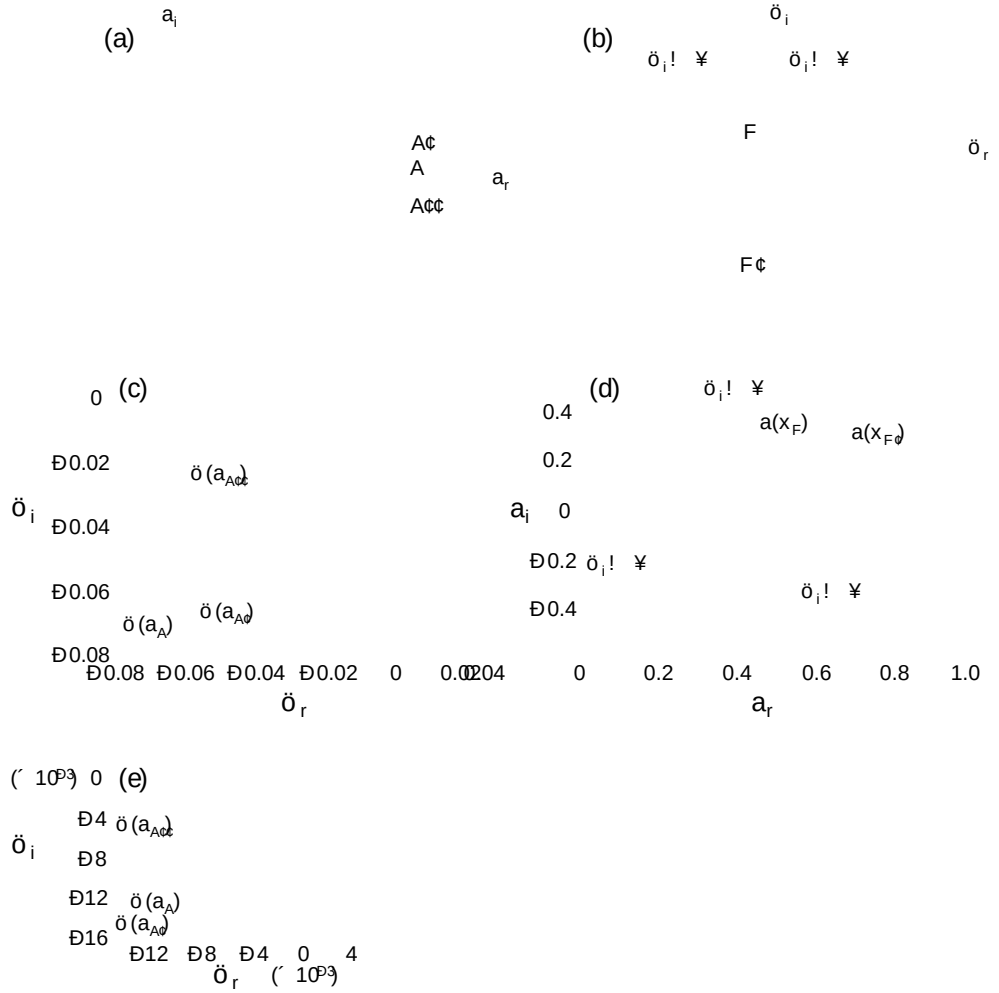

Figure 6. Paths in the - and ! -planes, (a) and (b), that map to branches in the! - and -planes in (c) and (d); (e) is an enlargement of (c). Re = 27:4, Ro = 1 and 0:1152, the zigzag lines in (a) indicate the imaginary-axis branch cuts, which begin at i = , and two branch points in the ! -plane and the corresponding values of (!) are depicted by and .

layer to stationary disturbances or to experimental measurement techniques that lter out travelling waves; see Lilly (1966, x5). Table 2 gives the values of Re, , and " at the noses of the marginal curves for stationary waves.

It has been shown in Lingwood (1995) that for Ro = 1 the branch point between branches 1 and 2, which lies close to the neutral-stability curve in gure 5 at Re 460, is not of pinch type and therefore does not cause an absolute instability. Figure 6

in figure 6(*d*). Both branch points are pinch points, because as $\omega_i \to \infty$ away from the branch points the mappings in the α-plane separate into distinct halves of the α-plane. That is, the branch points are a coalescence between two spatial branches: one that propagates energy outwards from the source and one that propagates energy inwards from the source. Furthermore, paths in the α-plane that pass through the pinch points form cusps at the branch points in the ω-plane. In general, when more than one pinch point exists, the one lying highest in the ω-plane dominates the time-asymptotic response. However, for these parameters ω_i^o is negative for both pinch points (only very slightly for the higher pinch point), therefore neither constitutes an absolute instability. The important point highlighted by figure 6 is that the behaviour of at least two branch points must be monitored as parameters are varied.

Marginal curves for absolute instability ($\omega_i^o = 0$) are given in various planes in figure 7 for Rossby numbers ranging from -1 to 1. Figure 7(*e*) is separated into two subplots for negative and positive Rossby numbers for clarity. Figure 7(*a*) shows the frequencies encompassed by the absolutely unstable regions. The dimensional frequency is $\omega^* = \omega Re \Omega^*$, where Ω^* is a constant, so waves propagating in r (or Re) retain constant values of $\omega_r Re$. As the Rossby number increases from -1, the critical Reynolds number for the onset of absolute instability Re_c decreases, the absolutely unstable region increases, and for $Ro \approx 0.5$ the onset occurs for stationary modes. For positive Rossby numbers, stationary modes tend to be close to the critical. But as $Ro \to -1$ the frequency of waves at Re_c becomes increasingly negative. Figure 7(*b*) shows only the $Ro = 1$ marginal curve and a second trajectory of branch points with $\omega_i = 0$. The nature of this second family of branch points is given in figure 8, which shows a selection of these branch points spanning a range of Reynolds numbers, and therefore having varying values of β. The broken lines show the separation of the two spatial branches involved in each branch point as $\omega_i \to \infty$ away from the value at the branch point. At $Re = 25$ and $Re = 28$ the branch points are of pinch type, which is consistent with figure 6 because there (where $Re = 27.4$) both branch points are pinch points. But for larger values of Re, the two spatial branches both separate into the lower half-α-plane, and therefore the branch points in this second family are no longer of pinch type and can be discounted from the description of the absolute unstable regions. The low-Reynolds-number pinch points in this second family have also been discounted because, for given β, the pinch points in the primary family become absolutely unstable at lower Reynolds number or, equivalently, for given β and Re the primary pinch points lie higher in the ω-plane. The absolutely unstable region is depicted in the (β, Re)-plane in figure 7(*c*) and the two families of branch points for $Ro = 1$ are given in 7(*d*). It becomes clear in figures 7(*e*) and (*f*) that by choosing the most critical curve of marginally absolutely unstable pinch points (rather than remaining on the continuous curve that becomes subcritical at $Re \approx 25$ and then, at larger Re, gives non-pinching branch points), a discontinuity is introduced into the curves for $1 \leqslant Ro \leqslant 0.9$. Figure 7(*g*) shows that, apart from the high-Reynolds-number part of the curves for $1 \leqslant Ro \leqslant 0.8$, the absolutely unstable region for flows with negative Rossby number lies in the lower half-α-plane, while the absolutely unstable region for flows with $Ro > 0$ lies in the upper half-α-plane . Thus, for $Ro < 0$, a spatial branch that originates in the upper half of the α-plane, i.e. an outwardly propagating mode, crosses into the lower half-plane, becoming convectively unstable before becoming absolutely unstable at a pinch point. For these flows, the qualitative instability behaviour is the same as that for the von Kármán layer, which is described in Lingwood (1995, 1996*a*). In general, for $Ro > 0$, a spatial branch that originates in the lower half of the α-plane, i.e. an inwardly propagating

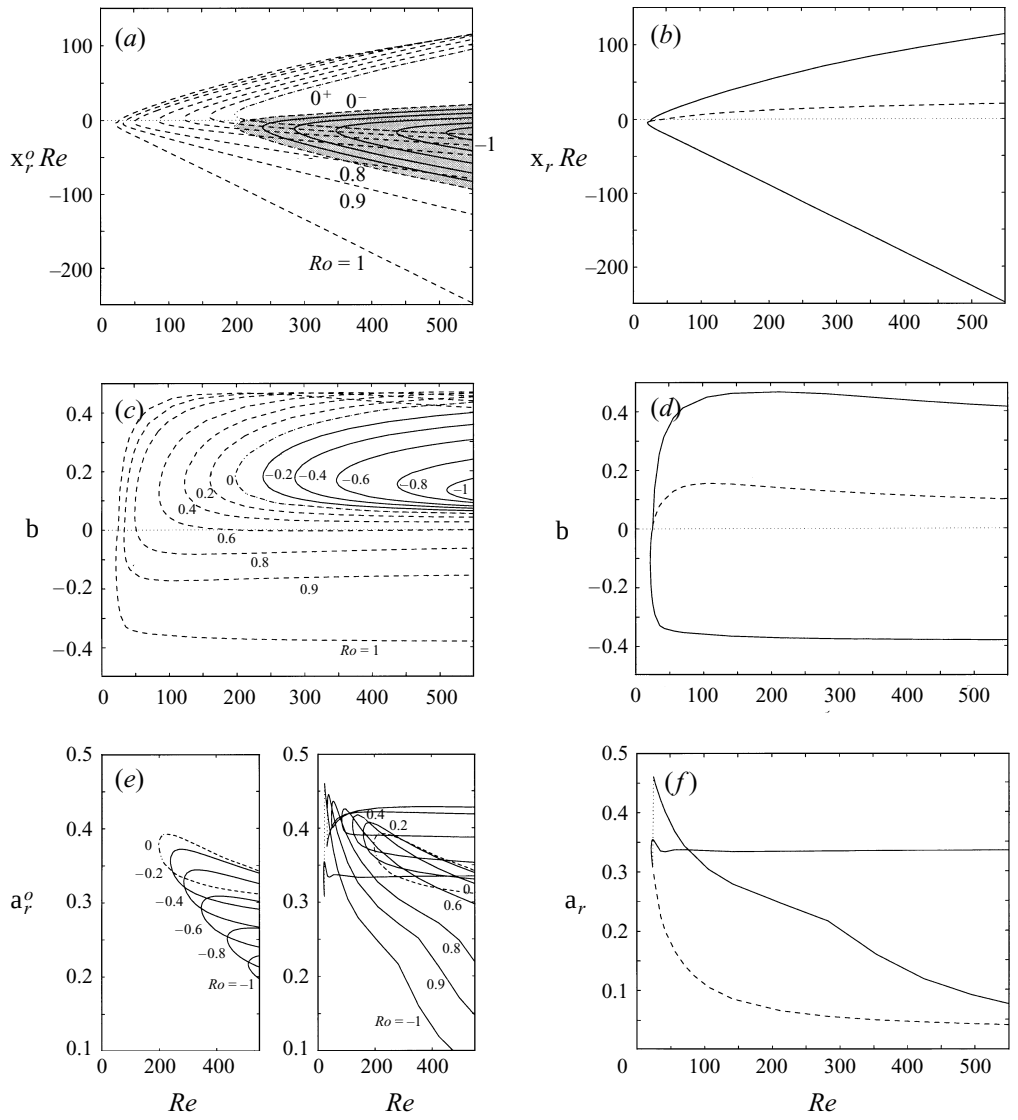

FIGURE 7 (*a–f*). For caption see facing page.

mode, crosses into the upper half-α-plane, becoming convectively unstable before coalescing with a spatially damped outwardly propagating mode at a pinch point and becoming absolutely unstable. However, for $1 \leqslant Ro \leqslant 0.8$ and high Reynolds numbers there are pinch points lying in the lower half-α-plane, which means that these flows with positive Rossby number then follow the description given above for flows with negative Rossby number. Since the Reynolds number for these pinch points is a lot higher than the critical value, this feature is not physically relevant because the absolute instability at lower Reynolds number will have already promoted the onset of nonlinearity and possibly laminar–turbulent transition. Finally, the wave angles for which the flows are absolutely unstable are shown in figure 7 (*i*).

Results from the inviscid analysis, i.e. using the Rayleigh equation, are presented in figure 9, where loci of the pinch points with varying β are given. The pinch points

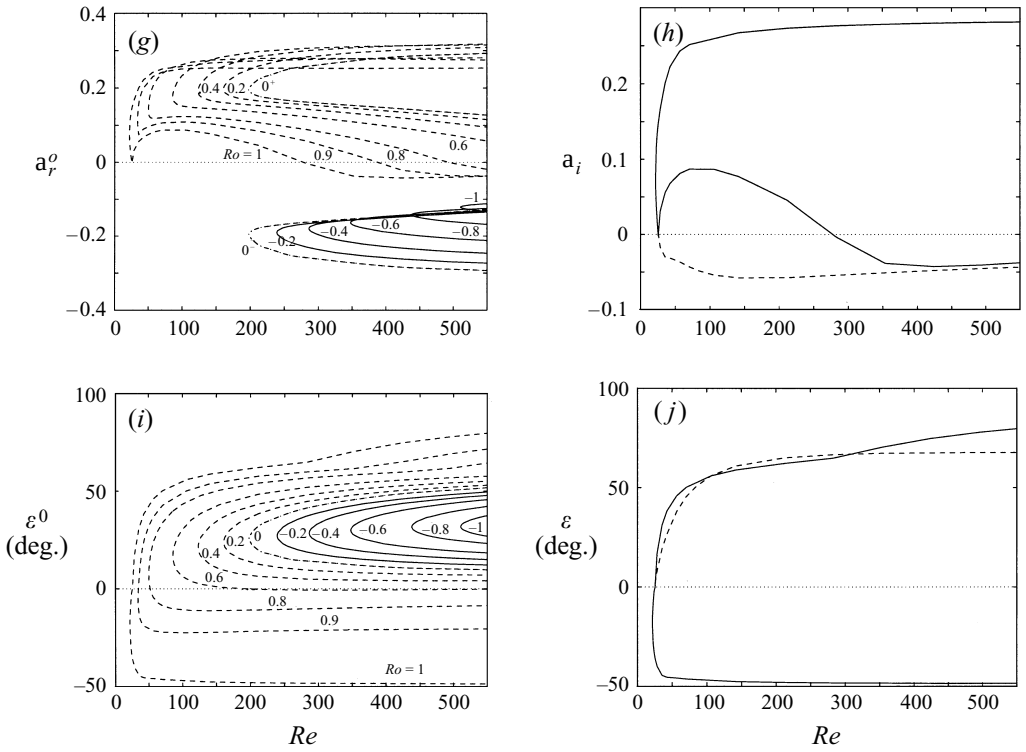

FIGURE 7. Marginal curves for absolute instability from the viscous analysis of the BEK system. The absolutely unstable regions ($\omega_i^o > 0$) lie within the curves. The shaded region in (*a*) highlights the curves for $-1 \leqslant Ro \leqslant 0^-$. In general, Ro is incremented by 0.2 from one curve to the next, apart from the inclusion of $Ro = 0.9$ in (*a*), (*c*), (*e*), (*g*) and (*i*). For $Ro = 1$, a second family of branch points with $\omega_i = 0$ (– – –) is shown in (*b*), (*d*), (*f*), (*h*) and (*j*).

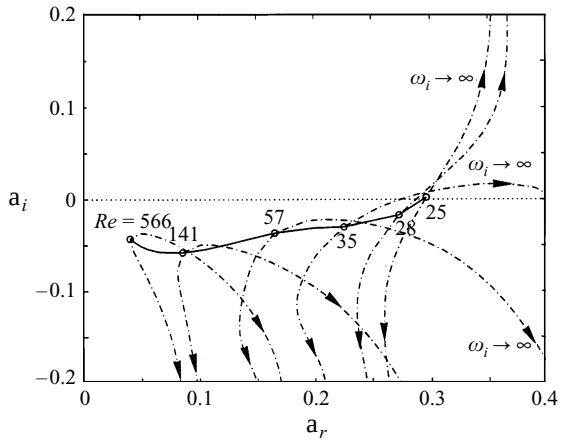

FIGURE 8. A selection of neutral ($\omega_i = 0$) family-2 branch points (○) given in the complex α-plane, showing the trajectories taken by the two separating spatial branches involved in each branch point as $\omega_i \to \infty$ (— · —).

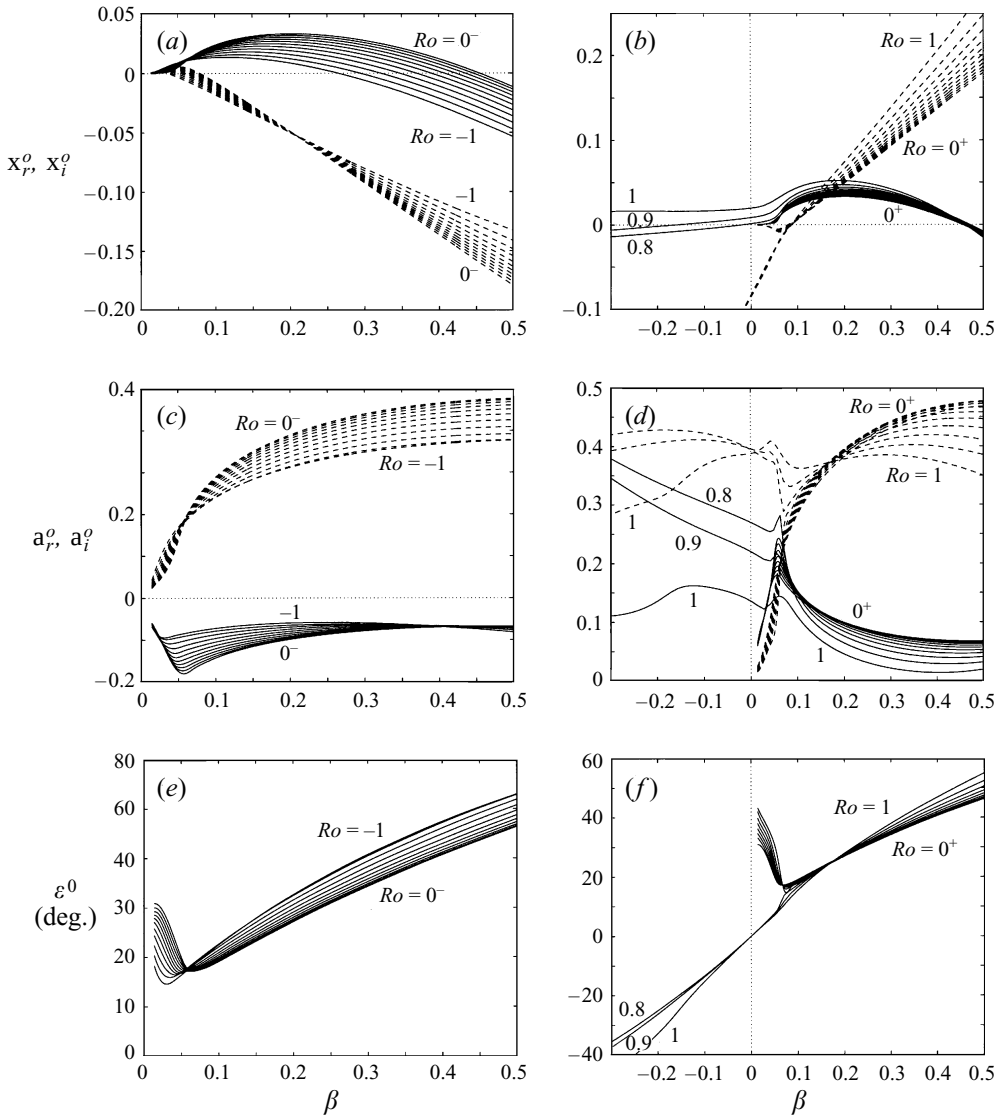

FIGURE 9. Loci of the inviscid pinch points ω_r^o (– – –) and ω_i^o (——) for varying β: (*a*) $-1 \leqslant Ro \leqslant 0^-$, (*b*) $0^+ \leqslant Ro \leqslant 1$. Inviscid loci of α_r^o (– – –) and α_i^o (——) for varying β: (*c*) $-1 \leqslant Ro \leqslant 0^-$, (*d*) $0^+ \leqslant Ro \leqslant 1$. Inviscid loci of ε^o for varying β: (*e*) $-1 \leqslant Ro \leqslant 0^-$, (*f*) $0^+ \leqslant Ro \leqslant 1$. In general, the Rossby number is incremented by 0.2 from one locus to the next, but with $Ro = 0.9$ included in (*b*), (*d*) and (*f*).

in the inviscid analysis occur between the asymptotic Reynolds-number limits of the branches involved in the pinch points in the viscous analysis. Where ω_i^o is positive the inviscid flow is absolutely unstable and the degree of absolute instability (the size of ω_i^o) is shown to increase with increasing Ro, as in the viscous analysis. The absolutely unstable range of β is very similar in the inviscid analysis to the range at large Reynolds numbers in the viscous analysis; see figure 7(*c*). In a comparable way to the absolutely unstable frequencies in figure 7(*a*), for $-1 \leqslant Ro \leqslant 0^-$ the inviscid absolutely unstable frequencies tend to negative values at the large-β limit,

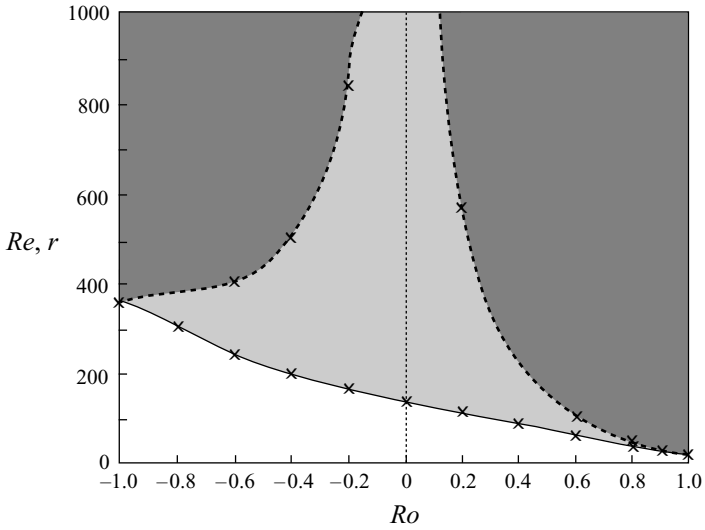

FIGURE 10. Critical Reynolds numbers (——) and radii (– – –) for the onset of absolute instability for the BEK system. The bounding lines are fitted to the calculated data points (×) and the shaded areas correspond to the absolutely unstable regions.

while approaching zero or becoming positive at small β. On the other hand, for $0^+ \leqslant Ro \leqslant 1$ the inviscid absolutely unstable frequencies tend to large positive values at the large-β limit, but become negative at small β. Furthermore, the inviscid results capture the branch-point behaviour at $Ro \approx 0.8$, which caused the jump from one Riemann sheet to another in the viscous analysis as the pinch points on one sheet first became subcritical to those on the other and then, through further branch switching, became non-pinching branch points. In the inviscid results there is a branch point in the loci of the pinch points at $Ro \approx 0.8$ and $\beta \approx 0.06$, which leads to the absolute instability persisting to negative β for $Ro \geqslant 0.8$ in the same way that the viscous absolutely unstable region in figure 7 (*b*) does. Although not shown in figure 9 (*b*), the negative-β limit of the inviscid absolutely unstable region for $Ro = 1$ is $\beta \approx -0.52$. Similar trends in α^o and ε^o are shown in figure 9 (*c–e*) as in the viscous analysis. The similarity between the viscous and inviscid absolute instability results is perhaps best illustrated by figure 4, which applies equally to the zero-Rossby-number solution of the BEK system as to the linear Ekman layer described in §2.

The onset of absolute instability, derived from the viscous analysis, for the various flows is summarized in figure 10. The solid line gives the critical Reynolds number for the onset of absolute instability as a function of *Ro* (with the lightly shaded part denoting the unstable region) and the broken lines give the critical radii for the onset of absolute instability, calculated from (3.19), as a function of *Ro* (with the darkly shaded part denoting the unstable region). Table 3 lists the approximate critical values for the onset of absolute instability (denoted by the subscript *c*).

For the BEK system, whether the Rossby number is positive or negative, the Reynolds number increases radially outwards. Thus, for flows with negative Rossby number, the laminar low-Reynolds-number region of the flow lies at small radii, convective instability of outwardly propagating waves occurs at higher Reynolds numbers (or larger radii), and the onset of absolute instability, which could promote nonlinearity and laminar–turbulent transition, occurs at a higher well-defined Reynolds number. It appears that the behaviour of all the negative-Rossby-number

Ro	Re_c	β_c	ω_c	α_c
−1.0	507.3	0.135	−0.0349	0.217−i0.122
−0.8	434.8	0.155	0.0393	−0.252−i0.142
−0.6	345.4	0.169	0.0418	−0.294−i0.164
−0.4	284.7	0.178	0.0425	−0.329−i0.180
−0.2	238.5	0.182	0.0413	−0.357−i0.191
$0.0^{\pm}$	198.0	0.184	$\pm$0.0397	0.379 $\pm$ i0.195
0.2	161.5	0.173	0.0314	0.393+i0.197
0.4	124.5	0.157	0.0199	0.403+i0.191
0.6	87.3	0.125	−0.00252	0.410+i0.176
0.8	51.4	0.0495	−0.0616	0.406+i0.141
0.9	34.5	−0.0417	−0.141	0.368+i0.118
1.0	21.6	−0.1174	−0.218	0.340+i0.0776

TABLE 3. Critical values for the onset of absolute instability in the BEK system.

flows is qualitatively similar to that of the von Kármán boundary-layer layer. Flows with positive Rossby number are more complicated. The low-Reynolds-number region of the flow again lies at small radii, but the radial mean velocity is now directed predominantly inwards (the axial mean flow is directed upwards) and the convective instability at higher Reynolds numbers is now of inwardly propagating, rather than outwardly-propagating, waves. From a purely convective viewpoint, this suggests that disturbances within the boundary layer grow as they are swept inwards but, provided their amplitudes are still sufficiently small, that they decay once they reach the stable Reynolds numbers at smaller radii. The onset of absolute instability in these positive-Rossby-number flows occurs at Reynolds numbers, and therefore radii, larger than those for the onset of convective instability (although they occur closer and closer together as the Bödewadt layer is approached). So, the general picture seems similar to that for flows with negative Rossby number: a laminar inner region, surrounded by a convectively unstable ring, surrounded by an absolutely unstable ring. However, the path of a particular disturbance is somewhat different. A disturbance initiated within the absolutely unstable region will grow in time at the initiation point (possibly triggering transition) and, assuming that the linear predictions are still useful, the spatial envelope associated with this temporal growth will excite the flow both inwards to and outwards from the source. Thus, the absolute instability may act as an exciter for inwardly propagating waves that pass out of the absolutely unstable and into the convectively unstable region and then into the stable low-Reynolds-number region. The history of a disturbance suggests a picture of relaminarization along its inward path.

Comparison between the absolute instability predicted by linear stability analysis and experimental observations for the von Kármán boundary layer are given by Lingwood (1995, 1996*a*). The onset of absolute instability was found to occur at $Re \approx 510$ (corrected here to about 507†) and the onset of transition is consistently found by various experimentalists (see Lingwood 1995) at an average value of 513 with only a 3% scatter around this value. Faller (1991), however, showed that transition of the von Kármán boundary layer is possible at lower Reynolds numbers via several nonlinear interaction mechanisms dependent upon the initial amplitude of

† In the course of this analysis, a small numerical error was found in the code used in Lingwood (1995). Here the critical Reynolds number for the onset of absolute instability for the von Kármán layer is corrected from 510.6 to 507.3.

excitation of type-2 disturbances by the free-stream flow. Presumably similar transition mechanisms could operate in the other members of the BEK system before the onset of absolute instability. The results presented here for the Ekman layer are applicable to the Ekman layers produced in low-Rossby-number experiments, e.g. Faller (1963), Tatro & Mollö-Christensen (1967) and Owen, Pincombe & Rogers (1985). In these experiments the Ekman layers were produced over a rotating disk with a source of fluid with radial velocity at the outer edge and a sink at the inner core (Owen *et al.* 1985 also studied the flow with the source at the centre and the sink at the outer edge). In this configuration, the fluid outside the boundary layer has a potential-vortex form, rather than fixed angular velocity, the radial flow is contained entirely within the boundary layer, and there is no axial mean velocity. The potential-vortex form implies that both the Rossby number and the Reynolds number are functions of radius, and both increase with decreasing radius. The turbulent region lies at smaller radius than the laminar region. Nevertheless, as the Rossby number tends to zero the mean flow in these source–sink-generated Ekman layers tends to the analytic solution for a linear Ekman layer described in §2, as does the zero-Rossby-number BEK flow, described in §3. The governing perturbation equations for these three cases also become exactly equivalent in the zero-Rossby-number limit. Most of the experimental studies of the laminar Ekman layer have concentrated on establishing the critical Reynolds number for convectively unstable waves and characterizing the instabilities as branch-1 or branch-2 modes; the onset of laminar–turbulent transition is not generally reported. However, Faller & Kaylor (1966) states $Re \approx 200$ as an approximate boundary between laminar and turbulent behaviour. Further, Owen *et al.* (1985) found that for $Re > 200$ and radial outflow in their source–sink flow, the circumferential velocity at large z departed from that predicted by linear theory for laminar flow and took this as the onset of turbulent behaviour in the Ekman layer. For both radial inflow and outflow they chose to define the onset of transition in the Ekman layers as $Re \approx 180$. These Reynolds number are close to the onset of absolute instability at about 198 in the Ekman layer. Further supporting evidence of the absolute instability in the Ekman layer is provided by Spooner & Criminale (1982), where the evolution of a wave packet generated by a pulsed disturbance in a linear Ekman layer is calculated using summation of discrete modes, including branch-1 and branch-2 modes. The group velocity (defined as the speed of the maximum of the wave packet) parallel and perpendicular to the geostrophic velocity is given for a range of Reynolds numbers. The group velocity of the branch-1 contribution to the wave packet decreases with Reynolds number, with the component perpendicular to the geostrophic velocity being only about 16.5% of the parallel component at $Re = 200$ (this is calculated by interpolating between the given data). Thus, the wave packet appears to propagate almost parallel to the geostrophic velocity, i.e. almost in the azimuthal direction in the BEK system. This is suggestive of an absolute instability in the direction normal to the geostrophic velocity, as found here, but the group velocities calculated by Spooner & Criminale (1982) would not be expected to tend to zero with the onset of absolute instability because they are defined, quite correctly, at the maximum of the spatial envelope of the wave packet, which is in general non-zero even in an absolutely unstable flow. Experimental observations of the instability of the Bödewadt layer do not seem to be available, perhaps because it is unstable to such low Reynolds numbers.

5. Conclusions

The linear Ekman layer and the family of boundary-layer flows established by a differential rotation rate between a disk and a fluid at infinity in rigid-body rotation (which includes the Bödewadt, the Ekman and the von Kármán boundary layers; the BEK system) have been investigated using linear stability theory. The general convective nature of much of each of these flows is already known, but this investigation has focused on the possibility of an absolute instability occurring in some parameter range. Given sufficient time, even a weakly absolutely unstable flow will cause a disturbance at a fixed point in space to grow to amplitudes large enough to make the use of linear theory invalid. In contrast, a disturbance in a convectively unstable flow is swept away as it grows, and the source area is ultimately left undisturbed, and so the boundary layer remains basically laminar until the instability wave has travelled far enough away to have grown to amplitudes sufficient to cause nonlinearities. Hence, absolute instability is quite distinct from spatial instability and is far more dangerous. In the absence of more dominant transition mechanisms, the absolute instability mechanism may explain the onset of nonlinearity and laminar–turbulent transition at a well-defined radial position in the BEK flows. Furthermore, the presence of an absolute instability would imply that any asymptotic stability analysis should be temporal as well as spatial.

In all cases, these flows have been found to be absolutely unstable in the direction normal to the free-stream velocity (the radial direction in the BEK system) above particular Reynolds numbers and for certain frequencies and wavenumbers of disturbance. For all but the Ekman layer ($Ro = 0$), which is parallel in the strict sense, the parallel-flow approximation has been used in the viscous analyses. Inviscid results are also presented that show in all cases that the absolute instability persists in the limit of large Reynolds number. This persistence implies that the viscous and Coriolis effects, which are both of order Re^{-1} and are therefore neglected in the Rayleigh equation, are not primary in causing the absolute instability. Unlike the viscous analyses, which in general employ the parallel-flow approximation and therefore are mathematically inconsistent to order Re^{-1}, the inviscid analyses are consistent and show that the absolute instability is not an artifact of the parallel-flow approximation. It is expected that the parallel-flow approximation will have some small numerical effect on the stability calculations, but that the general absolute instability characteristics discussed in this paper are still relevant to the physical behaviour of the flows, as has been shown for the particular case of the von Kármán flow (Lingwood 1995, 1996*a*) where the onset of transition and absolute instability coincide. There is also some experimental evidence (Faller & Kaylor 1966 and Owen *et al.* 1985) that the onset of transition in the Ekman layer occurs at $Re \approx$180–200, which is consistent with the onset of absolute instability at $Re \approx 198$.

For the von Kármán boundary layer the absolute instability always occurs for travelling (non-zero frequency) waves, but as the Rossby number is increased towards the Bödewadt boundary layer the stationary waves also become absolutely unstable. For the flow with $Ro \approx 0.5$ the stationary waves are the first to become absolutely unstable. The stationary waves are of particular importance because they are excited by unavoidable roughnesses on the surface of the disk, and are therefore often observed in experiments as so-called crossflow vortices. With the increasingly inflectional nature of the mean velocity profiles as $Ro \rightarrow 1$, the flows become increasingly unstable in both the convective and absolute senses; for the Bödewadt layer the onset of convective and absolute instability occurs almost simultaneously at very low Reynolds number.

For all the flows the absolute instability is caused by a pinch point between a spatially growing and a spatially damped branch of the dispersion relation. Apart from the special case where the pinch point lies on the real wavenumber axis, this must always be the case because in order for a branch point to be of pinch-type the two spatial branches that coalesce must originate in separate halves of the complex wavenumber plane for large positive imaginary frequency. In order to pinch, one of these branches must cross the real wavenumber axis, becoming convectively (spatially) unstable before pinching. So, the absolute instability always involves a branch of the dispersion relation that from a convective viewpoint is damped, and therefore uninteresting, and which has been ignored in previous studies for this reason. The absolute instability mechanism may be relevant to other three-dimensional boundary layers, for example the flow over swept wings; see Lingwood (1996*b*).

This work was performed while supported by a Research Fellowship at Pembroke College, Cambridge.

REFERENCES

Barcilon, V. 1967 On the motion due to sources and sinks distributed along the vertical boundary of a rotating fluid. *J. Fluid Mech.* **27**, 551–560.

Batchelor, G. K. 1951 Note on the class of solutions of the Navier–Stokes equations representing steady non-rotationally symmetric flow. *Q. J. Mech. Appl. Maths* **4**, 29–41.

Bers, A. 1975 Linear waves and instabilities. In *Physique des Plasmas* (ed. C. DeWitt & J. Peyraud), pp. 117–215. Gordon & Breach.

Bödewadt, U. T. 1940 Die Drehströmung über festem Grund. *Z. Angew. Math. Mech.* **20**, 241–253.

Briggs, R. J. 1964 *Electron-Stream Interaction with Plasmas,* chap. 2. MIT Press.

Ekman, V. W. 1905 On the influence of the earth's rotation on ocean currents. *Ark. Mat. Astr. Fys.* **2**, no. 11.

Faller, A. J. 1963 An experimental study of the instability of the laminar Ekman boundary layer. *J. Fluid Mech.* **15**, 560–576.

Faller, A. J. 1991 Instability and transition of the disturbed flow over a rotating disk. *J. Fluid Mech.* **230**, 245–269.

Faller, A. J. & Kaylor, R. E. 1966 Numerical study of the instability of the laminar Ekman boundary layer. *J. Atmos. Sci.* **23**, 466–480.

Gray, W. E. 1952 The nature of the boundary layer at the nose of a swept back wing. *Unpublished, Min. Aviation, Lond.*

Gregory, N., Stuart, J. T. & Walker, W. S. 1955 On the stability of three-dimensional boundary layers with application to the flow due to a rotating disk. *Phil. Trans. R. Soc. Lond.* A **248**, 155–199.

Healey, J. J. 1996 Characterizing boundary layer instability at finite Reynolds numbers. *J. Fluid Mech.* (submitted).

Henningson, D. S. & Schmid, P. J. 1992 Vector eigenfunction expansions for plane channel flows. *Stud. Appl. Maths* **87**, 15–43.

Hide, R. 1968 On source–sink flows in a rotating fluid. *J. Fluid Mech.* **32**, 737–764.

Huerre, P. & Monkewitz, P. A. 1990 Local and global instabilities in spatially developing flows. *Ann. Rev. Fluid Mech.* **22**, 473–537.

Kármán, Th. von 1921 Über laminare und turbulente Reibung. *Z. Angew. Math. Mech.* **1**, 233–252.

Koch, W. 1986 Direct resonance in Orr-Sommerfeld problems. *Acta Mechanica* **58**, 11–29.

Kupfer, K., Bers, A. & Ram, A. K. 1987 The cusp map in the complex-frequency plane for absolute instabilities. *Phys. Fluids* **30**, 3075–3082.

Lilly, D. K. 1966 On the instability of Ekman boundary flow. *J. Atmos. Sci.* **23**, 481–494.

Lin, C. C. 1945*a* On stability of two-dimensional parallel flows, Part I. *Q. Appl. Maths* **3**, 117–142.

Lin, C. C. 1945*b* On stability of two-dimensional parallel flows, Part II. *Q. Appl. Maths* **3**, 218–234.

Lin, C. C. 1945*c* On stability of two-dimensional parallel flows, Part III. *Q. Appl. Maths* **3**, 277–301.

Lingwood, R. J. 1995 Absolute instability of the boundary layer on a rotating disk. *J. Fluid Mech.* **299**, 17–33.

Lingwood, R. J. 1996*a* An experimental study of absolute instability of the rotating-disk boundary-layer flow. *J. Fluid Mech.* **314**, 373–405.

Lingwood, R. J. 1996*b* Absolute instability of swept boundary-layer flows. *J. Fluid Mech.* submitted.

Lingwood, R. J. 1997 On the application of the Briggs' and steepest-descent methods to a boundary-layer flow. *Stud. Appl. Maths* (in press).

Marlatt, S. W. & Biringen, S. 1994 On the spatial instability modes of the laminar Ekman boundary layer. *J. Atmos. Sci.* **51**, 3539–3542.

Marlatt, S. W. & Biringen, S. 1995 Numerical simulation of spatially evolving Ekman layer instability. *Phys. Fluids* **7**, 449–451.

Melander, M. V. 1983 An algorithmic approach to the linear stability of the Ekman layer. *J. Fluid Mech.* **132**, 283–293.

Owen, J. M., Pincombe, J. R. & Rogers R. H. 1985 Source–sink flow inside a rotating cylindrical cavity. *J. Fluid Mech.* **155**, 233–265.

Rogers, M. H. & Lance, G. N. 1960 The rotationally symmetric flow of a viscous fluid in the presence of an infinite rotating disc. *J. Fluid Mech.* **7**, 617–631.

Schlichting, H. 1979 *Boundary-Layer Theory*, 7th edn, pp 102–107, 225–230. McGraw–Hill.

Smith, N. H. 1947 Exploratory investigation of the laminar-boundary-layer oscillations on a rotating disk. *NACA TN* 1227.

Spooner, G. F. & Criminale, W. O. 1982 The evolution of disturbances in an Ekman boundary layer. *J. Fluid Mech.* **115**, 327–346.

Stewartson, K. 1957 On almost rigid rotation. *J. Fluid Mech.* **3**, 17–26.

Tatro, P. R. & Mollö-Christensen, E. L. 1967 Experiments on Ekman layer instability. *J. Fluid Mech.* **28**, 531–543.